AD_____

Award Number: W81XWH-€JËË€GGH

TITLE: Vಙ*^ಡ*ÁÚæ&|ãæ¢^|ËŠ[æå^åÁPæ}[]æ¢Œ|^•Á{ÁÚçæ¢ãæ}Á‸æ}&^¦

PRINCIPAL INVESTIGATOR:ÁÚ¢^]@ಇ}ÁÓÈÁP¸^||ËÁ‸ËÒÈ

CONTRACTING ORGANIZATION: University of Ôæ|ã{¦}ãæÁÚæ}ÁÓã*[
ÁŠæ¦R[||æÁÔŒÁJ€JHÁ

REPORT DATE: Tæ̂Á‸€FH

TYPE OF REPORT: Ü^çãã^åÁ‸]}æ|

PREPARED FOR: U.S. Army Medical Research and Materiel Command
Fort Detrick, Maryland 21702-5012

DISTRIBUTION STATEMENT: Approved for public release; distribution unlimited

The views, opinions and/or findings contained in this report are those of the author(s) and should not be construed as an official Department of the Army position, policy or decision unless so designated by other documentation.

REPORT DOCUMENTATION PAGE

1. REPORT DATE *(DD-MM-YYYY)*	2. REPORT TYPE	3. DATES COVERED *(From - To)*
May 2013	Revised Final	1 May 2009 - 30 April 2013

4. TITLE AND SUBTITLE

Targeting Paclitaxel-Loaded Nanoparticles to Ovarian Cancer

5a. CONTRACT NUMBER

5b. GRANT NUMBER
W81XWH-09-1-0223

5c. PROGRAM ELEMENT NUMBER

6. AUTHOR(S)
Stephen B. Howell

E-Mail: showell@ucsd.edu

5d. PROJECT NUMBER

5e. TASK NUMBER

5f. WORK UNIT NUMBER

7. PERFORMING ORGANIZATION NAME(S) AND ADDRESS(ES)

University of California, San Diego
La Jolla, CA 92093

8. PERFORMING ORGANIZATION REPORT NUMBER

9. SPONSORING / MONITORING AGENCY NAME(S) AND ADDRESS(ES)
U.S. Army Medical Research and Materiel Command
Fort Detrick, Maryland 21702-5012

10. SPONSOR/MONITOR'S ACRONYM(S)

11. SPONSOR/MONITOR'S REPORT NUMBER(S)

12. DISTRIBUTION / AVAILABILITY STATEMENT
Approved for Public Release; Distribution Unlimited

13. SUPPLEMENTARY NOTES

14. ABSTRACT

The specific aims of this project are to: 1) determine the efficacy, pharmacokinetics, toxicology and imaging capacity of RGD-targeted Nexil; and, 2) determine the ability of other ovarian cancer-specific targeting ligands to enhance the efficacy of Nexil. Substantial progress has been made on both of these specific aims. This is the final report. We have established that there is an excellent correlation between the tumor uptake of Nexil and its ability to deliver paclitaxel in a panel of 8 human tumor xenografts. Although we successfully synthesized RGD-target Nexil we were unable to show improved efficacy in a lung cancer mode. We have shown that the CPE peptide effectively targets the toxin gelonin to human ovarian cancer cells in a claudin-dependent manner, but that this fusion molecule has a difficult time getting out of the endosomal compartment and reaching the ribosome which is the target of gelonin. We have identified the A6 peptide as a CD44 tumor-targeting peptide worthy of further study.

15. SUBJECT TERMS
None provided.

16. SECURITY CLASSIFICATION OF:			17. LIMITATION OF ABSTRACT	18. NUMBER OF PAGES	19a. NAME OF RESPONSIBLE PERSON USAMRMC
a. REPORT U	**b. ABSTRACT** U	**c. THIS PAGE** U	UU	24	**19b. TELEPHONE NUMBER** *(include area code)*

Targeting paclitaxel-loaded nanoparticles to ovarian cancer
W81XWH-09-1-0223

Table of Contents

Title: Targeting Paclitaxel-Loaded Nanoparticles to Ovarian Cancer
Grant #: W81XWH-09-1-0223
Principal investigator: Stephen B. Howell, M.D.
Grant period: 5/1/09 – 4/30/12 (with no cost extension to 9/30/12)

INTRODUCTION

The **specific aims** of this project are to: 1) determine the efficacy, pharmacokinetics, toxicology and imaging capacity of RGD-targeted Nexil; and, 2) determine the ability of other ovarian cancer-specific targeting ligands to enhance the efficacy of Nexil. Substantial progress was made on both of these specific aims. This is the final report for this grant.

The success of Abraxane in increasing the delivery of placitaxel (PTX) to breast cancers has sparked interest in other nanoparticle-based delivery systems that might out-perform Abraxane. CT-2103 (Xyotaq) consists of a polyglumatic acid (pGA) polymer to which PTX has been loaded to 37 %(w/w). This drug has proven safe, but has not yet been shown to have improved efficacy in phase 3 trials. We have further improved on CT-2103 by modifying the pGA backbone such that each glutamic acid in the polyer has an additional glutamic acid linked to as a side chain (pGGA). This polymer can also be loaded to a high level with PTX (35%); however, the key advantage is that the pGGA polymer loaded with PTX (pGGA-PTX) spontaneously forms a 20 nm particle in aqueous solutions and plasma. This molecule, now known as Nexil[TM], increased plasma exposure by 24-fold over that attainable with an equimolar dose of free PTX, and in the H460 lung cancer model it increased delivery of PTX ($AUC_{0-\infty}$) by 68-fold [1]. We have now shown that Nexil significantly outperforms both free paclitaxel and Abraxane with respect to efficacy in multiple tumor [2].

The rationale for attaching tumor-targeting ligands to Nexil derives from the very large increase in affinity attained when multiple ligands work together to produce a Velcro-like effect. While the association rate constant increases linearly with the number of ligands, the dissociation rate falls exponentially such that the overall affinity increases markedly. The affinity can become so high that, once the dendrimer is bound, it cannot be displaced even by very high concentrations of the free ligand.

BODY

Background

Despite of the improvements in the cancer treatment concerning surgical intervention, radiation and chemotherapeutic drugs, development of efficient delivery of therapeutic systems is lagged behind. This subject has been actively reviewed and it is of common agreement that nanotechnology represents an excellent opportunity to move forwards the drug delivery research [3-6].

Among the systems currently being investigated, the polymeric nanoparticles conjugates have already demonstrated promising application [4]. These macromolecular prodrugs comprise a minimun of three components: a natural or synthetic water-soluble polymeric carrier, a biodegradable polymer-drug linkage and bioactive antitumor agent. In this sense, a polyglutamate polymer loaded with paclitaxel (CT-2103, Xyotax) was described in 1998 with good *in vivo* antitumor activity [7]. However, although favorable phase II clinical trial results, three randomized phase III trials in patients with non-small cell lung cancer failed to demonstrate an improvement in either progression-free or overall survival and CT-2103 has not yet received marketing approval.

Based on a polyglutamic acid polymer backbone, we have developed a new polymer where a glutamate side chain has been added to each monomer in the polymer to create polyglutamylglutamate (PGGA). When PTX is conjugated to this polymer to an extent of 35% (w/w) to create poly-(_-L-glutamylglutamine)–paclitaxel

(PGGA–PTX), the tendency of the hydrophobic PTX molecules to interact with each other causes the polymer to collapse to form a nanoparticle of ~20 nm in aqueous solutions as determined by dynamic light scattering [2, 8] (Figure 1).
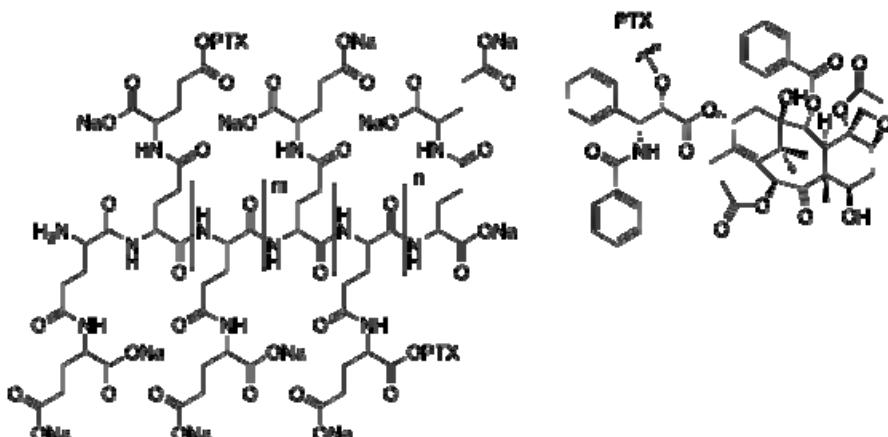

Figure 1

In our studies, this new nanoparticle, now called Nexil, has exhibited better efficacy compared to Abraxane (clinically approved paclitaxel formulation) and better pharmacokinetic parameters compared to native paclitaxel [1, 2]. It is very likely that the advantage of Nexil is based on its ability to passively target to the tumor due to its abnormal vasculature. Passive targeting exploits the "enhanced permeability and retention" (EPR) effect that allows nanocarriers to accumulate in the tumor. However, it is very desirable that drug delivery systems (DDS) also actively target to cancer cells. In principle, this active approach could be performed by conjugating DDS with molecules that bind to receptors specifically over-expressed on the target cells.

The **overall goal** of this research project is to further enhance the therapeutic efficacy of Nexil by targeting it to either the activated endothelial cells in tumors for anti-angiogenesis therapy, or to tumor cells themselves using peptides. The peptide chemical space is enormous and peptides are versatile in structure and conformation and highly pure peptides can be synthesized in large quantities compared to the protein ligands. Peptide ligands also generally display higher affinities for target receptors than the small molecule ligands. Although the Nexil nanoparticles are already extensively and rapidly endocytosed by tumor cells, our **hypothesis** is that selectively can be substantially further improved using the capability of the pGGA polymer to carry a large number of tumor-specific peptides per molecule. Our present goal is to combine this novel polyglutamylglutamate nanoparticle containing paclitaxel with the known cyclic peptide (RGD) and with the tumor penetrating peptide Lyp-1. The RGD peptide exhibits good binding affinity to $\alpha_v\beta_3$ integrins which are over-expressed in tumor cells, and Lyp-1 binds to p32 found in high levels in a subset of ovarian cancer. Thus, it is expected that this new system would be able to deliver its payload (paclitaxel) to tumor cells in a very selective manner.

Specific Aim #1: Determine the efficacy, pharmacokinetics, toxicology and imaging capacity of RGD-targeted Nexil

1. Correlation between the delivery by NEXIL-DTPA of ^{111}indium and ^{3}H-paclitaxel in human tumor xenografts

Our previous studies had established that Nexil out-performs Abraxane in multiple tumor models with respect to inhibition of tumor growth [1, 2]. As a first step toward the targeting of Nexil with peptides we wished to determine the relationship between the accumulation of the drug delivery system itself and the accumulation in the tumor of the paclitaxel. To this end we synthesized a form of Nexil that is conjugated with DTPA that

allows loading with ^{111}In that could be used to amount of the Nexil backbone accumulating in the tumor. This form of Nexil could also potentially permit ex vivo imaging of the amount of Nexil that accumulates in the tumor and this might be used to select patients for treatment with Nexil in future clinical trials.

The objective of this experiment was to determine whether there is a correlation between the amount of ^{111}In and the amount of [3H]-paclitaxel reaching the tumor when tested in 8 different human tumor xenografts. Female nu/nu mice were inoculated SC with 4×10^6 of each of 8 different human tumor cell lines of different histologic type. Any give mouse received inoculations on each shoulder and each hip and thus carried 4 different types of tumor. At the point when the mean tumor volume for the entire population reached 400 mm^3 (6 – 7 mm diameter) each mouse received a single IV bolus injection of [3H]-Nexil-DTPA-[111]In. Four hours later blood was obtained by cardiac puncture, the mice were sacrificed and the tumors dissected free of subcutaneous tissue. Each tumor was weighed and then placed in a vial and the ^{111}In dpm was counted on a gamma counter. The tumor sample was then be homogenized, mixed the scintillation fluid and the [3H] dpm were determined on a scintillation counter.

Twelve nu/nu mice were divided into two groups of 6 mice each. The mice in the first group were inoculated with 0.1 ml of the cell suspension in Matrigel as follows on 10/14/2010:

    Left shoulder: 2008 cells
    Right shoulder: A2780 cells
    Left hip: IGROV-1 cells
    Right hip: HEY cells

The mice in the second group were inoculated with inoculated with 0.1 ml of the cell suspension in Matrigel as follows on 10/14/2010:

    Left shoulder: KF28 cells
    Right shoulder: UCI 107 cells
    Left hip: H460 cells
    Right hip: HCT116 cells

All 12 mice were injected [111]Indium labeled [3H]-Nexil-DTPA on 11/2/2010 and sacrificed 4 hours after injection. The amount of indium in each tumor and plasma sample was determined using a gamma counter and the percent of the injected dose was calculated according to the standard assumptions as to blood volume. The amount of indium in each tumor was expressed as % ID/g (percent of injection dose per gram of tumor). The data tables are included in this report as appendices. Approximate 15% of injected dose was found in the plasma in group 1 and 10 % of injected dose was detected in plasma in group 2. The large error in group 2 was because one mouse died right after anesthesia. Therefore, we had difficulty doing a cardiac puncture; some blood was obtained after opening the chest, but it was mixed with other tissues and blood and led to the high cpm count. Nevertheless this value was included that in the calculation.

Approximately 2 % of injected indium dose per gram detected in HEY, which was the highest, followed by IGROV-1, HCT116 and 2008.
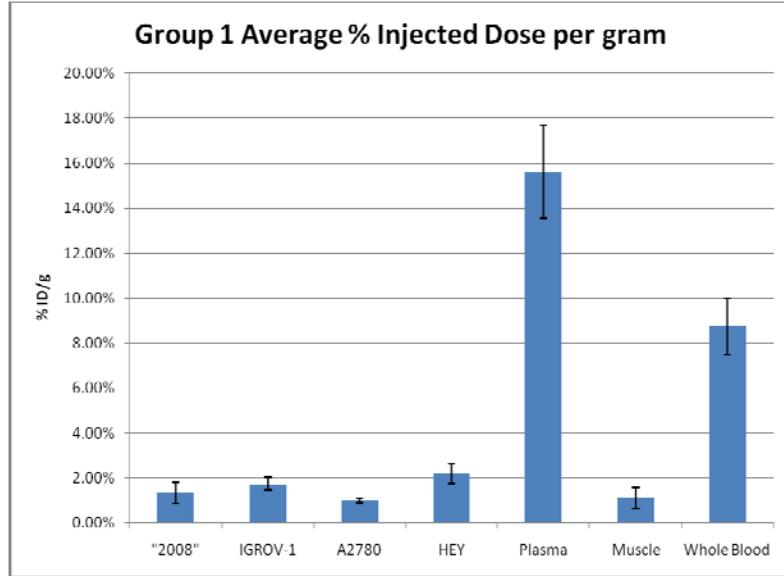
***Figure 2***. *Average % injected dose per gram in group 1. Vertical bars, ± SD*
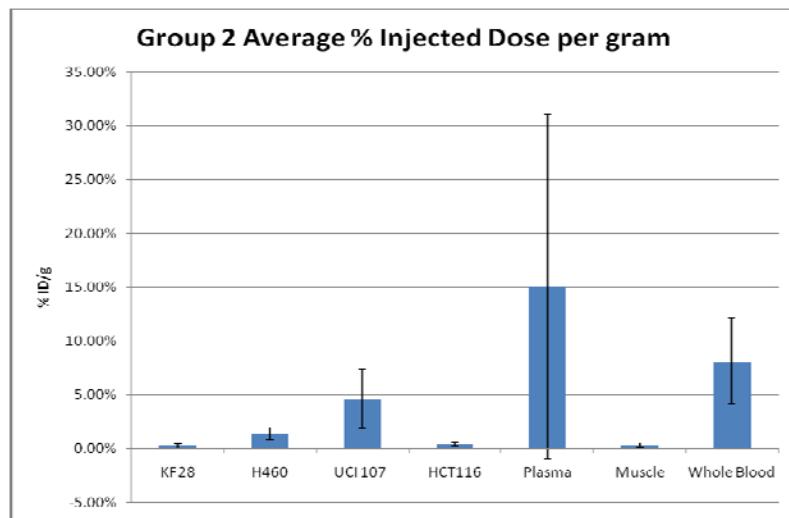
***Figure 3***. *Average % injected dose per gram in group 2. Vertical bars, ± SD.*
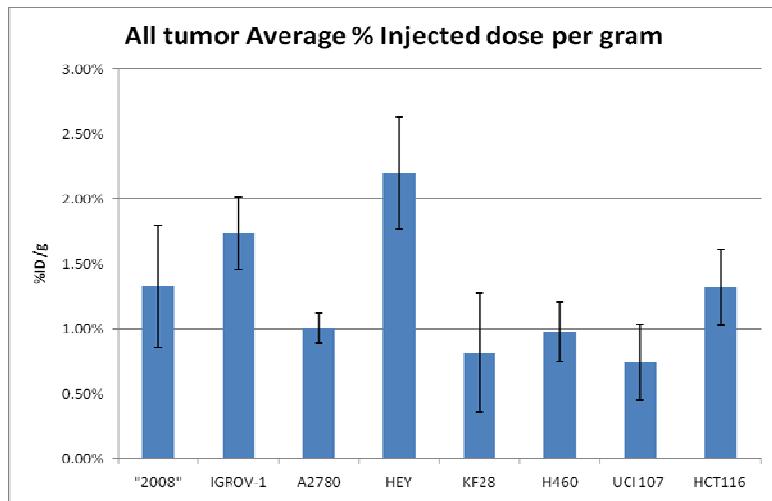
Figure 4. *Average % injected dose per gram for tumors in groups 1 and 2 combined. Vertical bars, ± SD*

Each tumor sample was then homogenized, mixed the scintillation fluid and the ^{3}H dpm was determined on a scintillation counter. The amount of [^{3}H]-paclitaxel in each tumor was expressed as DPM/g tumor (Figure 5). HEY also has the greatest tritium count, followed by IGROV-1, HCT116 and 2008.
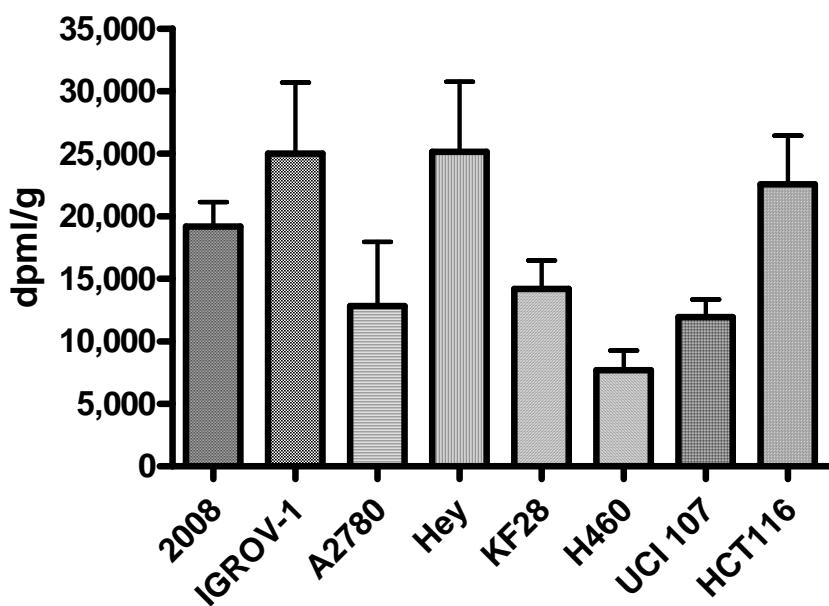
Figure 5. *Average of the amount of [^{3}H]-paclitaxel/g in all tumors. Vertical bars, ± SEM*

Figure 6 shows a scattergram of the ^{111}indium and ^{3}H counts per gram of weight for each of the 8 types of tumors. The correlation coefficient (r) for the delivery by Nextil-DTPA of ^{111}indium and [^{3}H]-paclitaxel across the 8 different tumor types was 0.853 (t = 4.009, p <0.01).
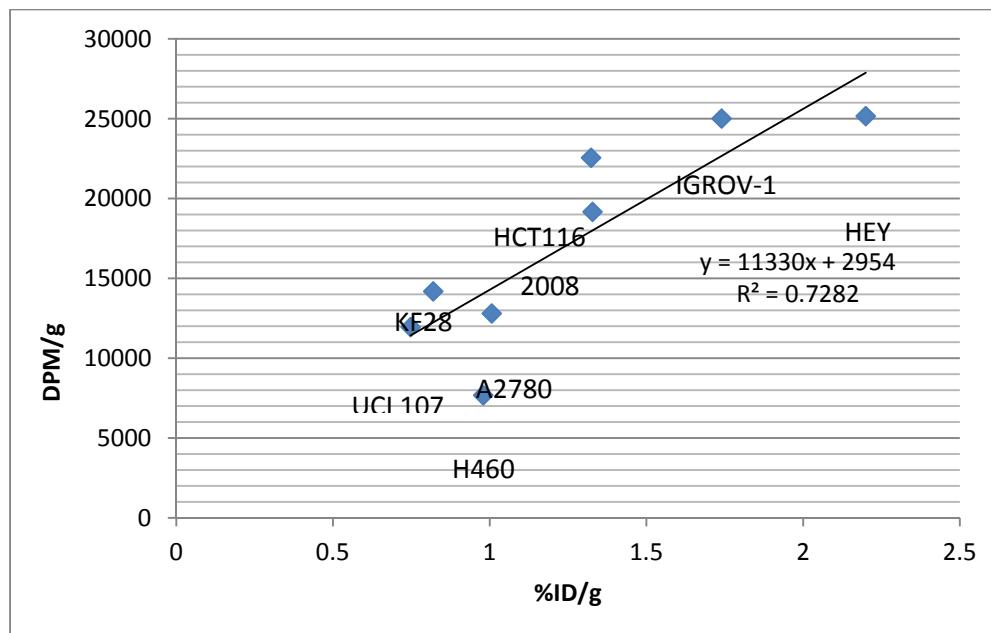
Figure 6. *Correlation between the delivery by Nextil-DTPA of ^{111}indium and [^{3}H]-paclitaxel*
Each data point represents the mean of values for 6 mice. ^{111}Indium counts are shown on the abscissa and [^{3}H] counts on the ordinate.

The data from this experiment disclosed several important points about the behavior of Nexil. First, it is clear that there are substantial differences in the accumulation of Nexil in different types of tumors when measured at 4 hours after IV injection. Among the 8 different tumors tested in this experiment there was a >3-fold variance in the accumulation of [^{3}H]-paclitaxel and >20-fold variance for the accumulation of ^{111}indium. Assuming that there is a relationship between the amount of Nexil that accumulates in a tumor and the probability of response, there is thus a clear opportunity to use trace injections of Nexil-DTPA as a tool with which to select patients for treatment with Nexil.

A second important point is that there was a very good correlation between the accumulation of ^{111}indium and [^{3}H] paclitaxel across the panel of the 8 different tumors used in this study. The correlation coefficient was 0.853. Thus, we can conclude that when both radioactive labels are on the same polymer, when a high accumulation of the ^{111}indium is accompanied by a high accumulation of paclitaxel. This observation suggests that the accumulation of Nexil-DTPA, which can be quantified in patients using a gamma camera, is a valid surrogate measure of the ability of Nexil to deliver paclitaxel to the tumor.

In the current experiment the [^{3}H]-paclitaxel and the ^{111}indum labels were on the same Nexil molecules. To further validate Nexil-DTPA as a tool with which to select patients for treatment with Nexil in clinical trials, it would be helpful to repeat this experiment injecting a mixture Nexil-DTPA loaded with ^{111}indium and [^{3}H]-paclitaxel-Nexil with the two labels on separate Nexil molecules.

2. *Comparison of the Tumor and Plasma Pharmacokinetics of Nexil and RGD-Conjugated Nexil*

As detailed in the Annual Reports for the first two years of this grant, we succeeded in synthesizing the RGD peptide and conjugating it to the Nexil backbone (15 RGD per polymer) in an attempt to target it to tumor and tumor endothelial cells expressing activated integrins. The goal of this experiment was to determine whether RGD-conjugated Nexil accumulates to higher levels in human lung carcinoma H460 xenografts than unconjugated Nexil.

A total of 48 female nu/nu mice were inoculated SC with 4×10^6 H460 lung cancer cells at 4 sites (left and right shoulder and left and right hip). At the point when the mean tumor volume for the entire population reached 400 mm^3 (6 – 7 mm diameter) the mice were randomly allocated into two groups of 24. Mice in group 1 received a single IV bolus injection of [^{3}H]PTX-Nexil and mice in group 2 received a single IV bolus injection of [^{3}H]PTX-Nexil-RGD. At 10 minutes and 1, 4, 12, 24, 48, 96 and 192 h after injection 3 mice from each group were sacrificed. Blood was obtained at the time of sacrifice, and after sacrifice the tumors were dissected free of subcutaneous tissue. Each tumor was weighed, homogenized, mixed with scintillation fluid and the ^{3}H dpm were determined on a scintillation counter. A graph was constructed of plasma and tumor concentrations of total [^{3}H]PTX as a function of time.

Plasma concentration of [^{3}H]PTX

Forty-eight mice were randomly allocated into 2 groups. Mice in group 1 received a single IV bolus injection of [^{3}H]PTX-Nexil and mice in group 2 received a single IV bolus injection of [^{3}H]PTX-Nexil-RGD. Blood samples were collected at 0.16, 1, 4, 12, 24, 48, 96, 192 hours after injection. One hundred µL of plasma was collected, transferred to scintillation vials and counted on a scintillation counter. The amount of [^{3}H]-paclitaxel in each plasma sample was expressed as DPM/g plasma. As shown in Figure 6, over the first 4 h there was a trend toward a lower plasma tritium concentration in the mice injected with [^{3}H]PTX-Nexil-RGD. There was a statistically significant difference in the plasma concentrations at 0.16 (p =0.048) and 4 h (p = 0.0252) using two-tailed paired *t* test for unpaired samples in the GraphPad Prism4 software. The area under the concentration-times-time curve for [^{3}H]PTX-Nexil-RGD was 56.2% of that for [^{3}H]PTX-Nexil.
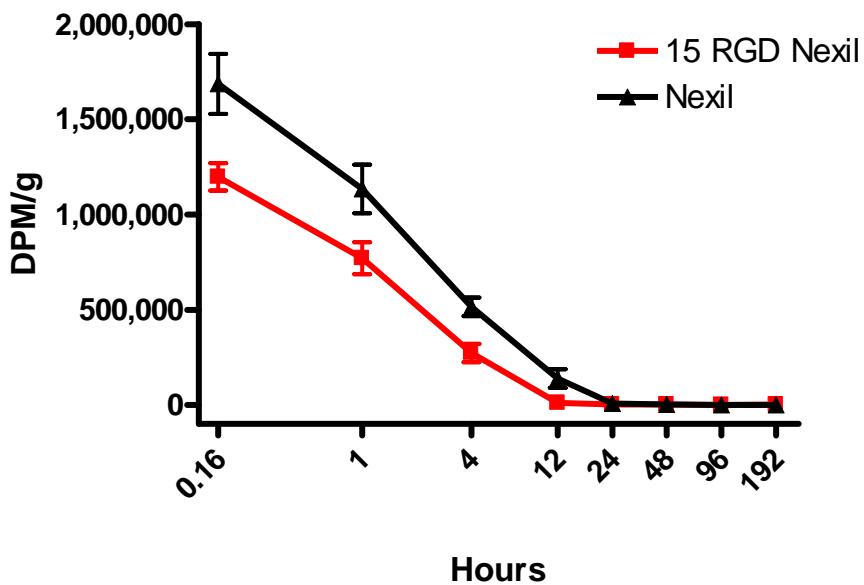
Figure 7. *[³H]PTX levels in plasma. Each point represents the mean of three plasma samples from three mice.* ■: *Mice treated with 15 RGD Nexil;* ▲: *Mice treated with unconjugated Nexil; Points: Mean ± SEM.*

Tumor concentration of [³H]PTX

Tumors were collected at 0.16, 1, 4, 12, 24, 48, 96, 192 hours after injection from the same 48 mice in which plasma had been collected. Samples were homogenized and counted on a scintillation counter. The amount of [³H]-paclitaxel in each tumor sample was expressed as DPM/g tumor. Among 4 tumors from each animal, the most obvious outlier was removed from each group. The average of [³H]-paclitaxel from the remaining three tumors in any given mouse was calculated and plotted in Figure 7 as a function of time and treatment. There was a statistically significantly higher tumor content of [³H]PTX-Nexil rather than [³H]PTX-Nexil-RGD at 24 ($p = 0.02$) and 96 h ($p = 0.02$). The area under the content-times-time curve for [³H]PTX-Nexil-RGD was 60.4 % of that for [³H]PTX-Nexil.
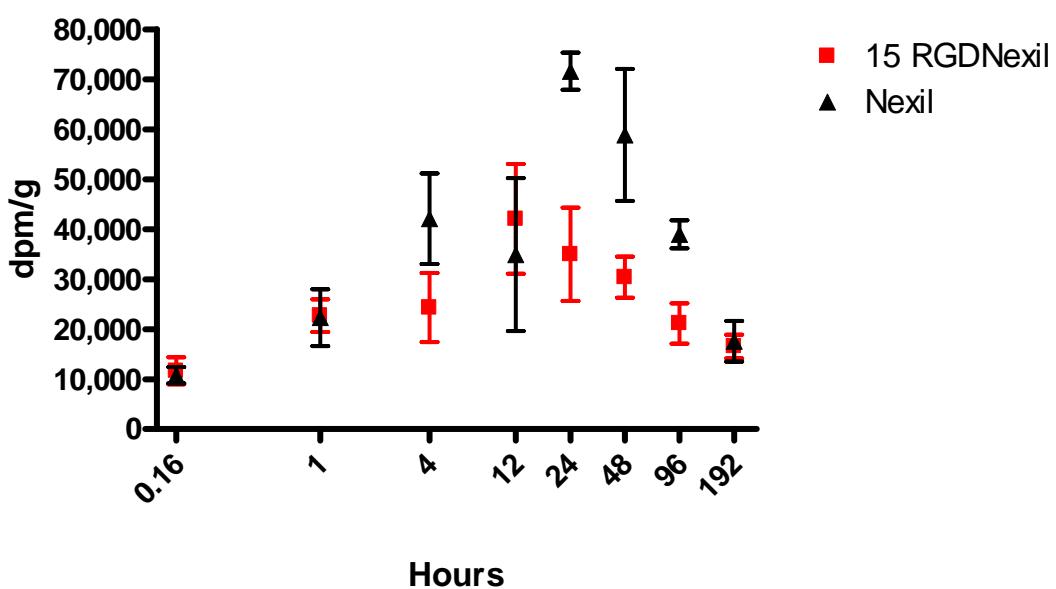

Figure 8. *[³H]PTX levels in tumors. Each point represents the mean of 3 mice.* ■: *Mice treated with 15 RGD Nexil;* ▲: *Mice treated with unconjugated Nexil; Points: Mean ± SEM.*

The RGD peptide has good binding affinity to activated $\alpha_v\beta_3$ integrin receptors which are commonly expressed on the endothelial cells of tumors and often on the tumor cells themselves. It was expected that addition of 15 cyclic RRD peptides per Nexil polymer would increase the delivery of paclitaxel to tumors in a selective manner. However, the RGD-conjugated Nexil did not perform any better than the Nexil itself. RGD-Nexil reached a lower maximum plasma concentration than Nexil when measured at 0.16 h after injection and this trend toward lower plasma concentration continued for the first 4 hours after injection. Interestingly, there was no corresponding difference in the tumor content of RGD-Nexil and Nexil during the same period. Using just the exponential phase of the plasma decay curve over the first 12 h, the half-life of the RGD-Nexil was estimated to be 1.6 h and that for Nexil 1.9 h.

The tumor content of tritiated paclitaxel reached a peak at 24 h following injection of Nexil and at 12 h following injection of RGD-Nexil. The maximum peak tumor content for RGD-Nexil (at 12 h) was only 59.2 % of that for Nexil at 24 h. Following the peak content, the washout of RGD-Nexil and Nexil was similar. Non-linear regression estimated the washout half-life to be 78 h for RGD-Nexil and 82 h for Nexil.

To provide further insight into the effect of adding 15 RGD per Nexil to the performance of Nexil, the cytotoxicity of Nexil was compared to that of RDG-Nexil in two cell line model systems. The first consisted of an isogenic pair of human melanoma cell lines one of which expresses the αV integrin (M21) and the other of which does not (M21L). The second consisted of the human lung carcinoma cell line H460. As shown in Figure 8, there was no significant difference in the cytotoxicity of RGD-Nexil against either the αV-expressing or αV non-expressing melanoma cell line, suggesting that the RGD loaded onto Nexil was not capable of engaging integrin receptors in a manner that resulted in greater paclitaxel delivery into the cells in tissue culture. The IC_{50} for the M21 cells was 0.53 µM and for the M21L line it was 0.74 µM.
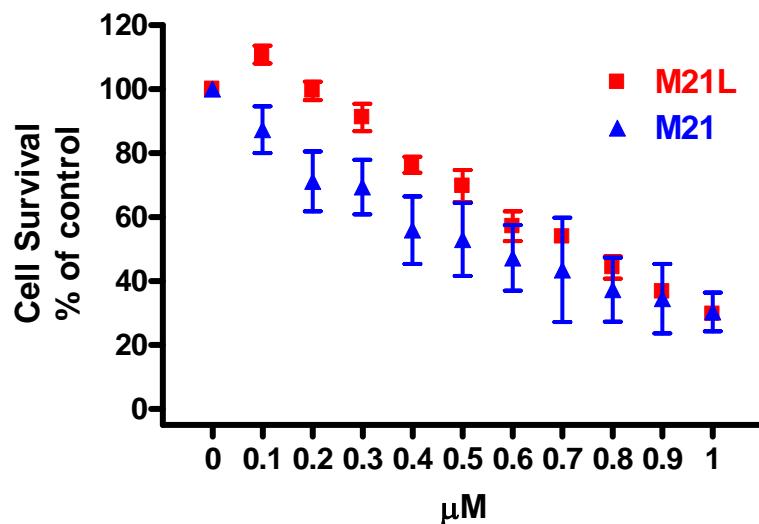
Figure 9. The CCK8 assay was used to assess the cytotoxicity of RGD-Nexil against an isogenic paired of human melanoma cells one of which expressed the αV integrin (M21) and the other of which did not (M21L). Both types of cell were exposed to drug for 72 hours. OD 450 nm was measured using a microplate reader. Points, mean of at least three experiments each performed with triplicate cultures.

As shown in Figure 10, RGD-Nexil was somewhat less toxic to H460 cells in vitro than Nexil. The IC_{50} value for Nexil was 0.6 µM; that for RGD-Nexil was clearly greater but could not be calculated from the data available.
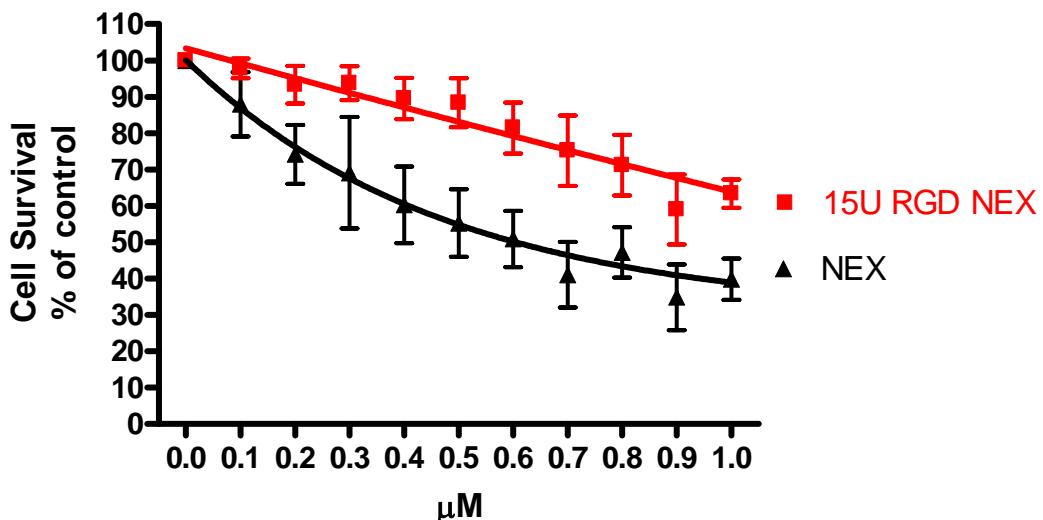
Figure 10. *The CCK8 assay was used to measure assess the cytotoxicity of Nexil and RGD-Nexil against the H460 lung cancer cell line in a 72 h assay. OD 450 nm was measured using a microplate reader. Points, mean of at least three experiments; each done in triplicate)*

These experiments documented that RGD-targeted Nexil was not achieving a degree of tumor specific targeting to make it of substantial interest for further pharmaceutical development. Thus, we turned our attention to Specific Aim #2, the identification and investigation of other tumor targeting ligands that might have greater potential for delivering Nexil or other payloads to ovarian carcinoma cells.

Specific Aim #2: Identification of additional molecules capable of targeting to ovarian cancer

1. *Lyp-1 targeting*

Lyp-1 is a member of a novel class of peptides that can markedly and selectively increase the penetration of drugs into tumor nodules [9]. Lyp-1 was originally isolated from a phage display library on the basis of its ability to direct phage to MDA-MB-435 tumor xenografts. [10] This compound has proved to bind specifically to tumor lymphatic and tumor cells, leading to cell death by apoptosis and inhibiting tumor growth in mice bearing breast cancer xenografts. The attractive feature of Lyp-1 is the ability of this compound to be internalized by tumor cells, which can be explored for drug delivery purposes.[11] Recently, Ruoslahti et al have suggested the internalization mechanism of Lyp-1 is through the known receptor p32 that is present and overexpressed at the tumor cell surface [12].

Our goal in was to synthesize Lyp-1 and use it to enhance targeting of Nexil to tumors (Figure 11).
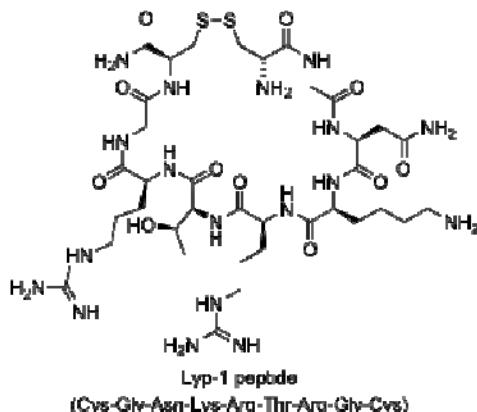
Figure 11. Structure of the Lyp-1 peptide

Precedents in the literature supported our hypothesis that the efficacy of Nexil coud be further improved using Lyp-1 as targeting moiety. Nanoparticles of iron oxide,[13] albumin-based [14] and even baculovirus combined with Lyp-1 have demonstrated excellent results for binding tumor cells [15].

Lyp-1 linker

Due to an important lysine residue in the Lyp-1 structure, the linkers we had previously designed and synthesized for the RGD peptide could not be used for the conjugation with the Nexil backbone. The Lyp-1 peptide requires a linker with an orthogonal reactivity towards the different amino acids residues present in the peptide. The maleimide group and/or azido group met this condition for the conjugate synthesis. The maleimide group presents excellent selectivity for sulfhydryl functionalities present in the cysteine or cysteine derivatives. On the other hand, the azido group can react with alkyne functionality (click chemistry) being widely used for conjugation purpose by several groups.

As reported in the annual reports the synthesis of the linker for the Nexil-Lyp1 conjugate was successfully accomplished as depicted in the Scheme 1.
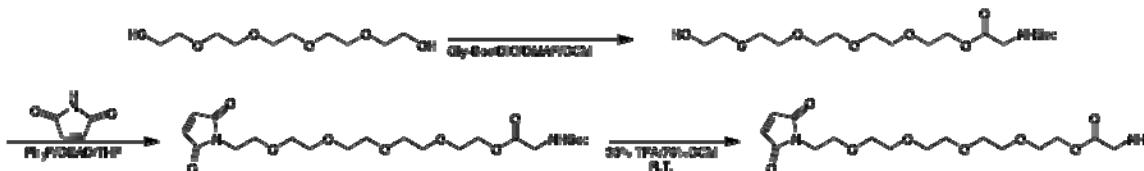
Scheme 1

The final compound was obtained after deprotection of the Boc group using a solution of TFA (30%) in dichloromethane at room temperature. The solvent was evaporated in the rotavaporator and the crude obtained was dissolved in water and washed 2 times with a solvent mixture of hexane(70%)/ethyl acetate (30%). The aqueous phase was lyophilized providing the desired compound with excellent yield (94%).

Nexil-Lyp-1 linker synthesis

As mentioned previously, the Lyp-1 structure contains an important lysine residue that hampers the synthesis of the conjugate using the same protocol described for RGD peptide. Moreover, the required maleimide group for thiol conjugation is very sensitive under basic conditions, which presented an additional challenge due to the inability to purify the product by dialysis.

We found that the synthesis of Lyp-1 conjugate had to be performed in two steps. The first step is the synthesis the Nexil-Lyp-1 linker using the activated Nexil and the Lyp-1 linker. The second step is the conjugation between the Lyp-1 peptide and Nexil-Lyp-1 linker.

First Step- Nexil Lyp-1 linker coupling
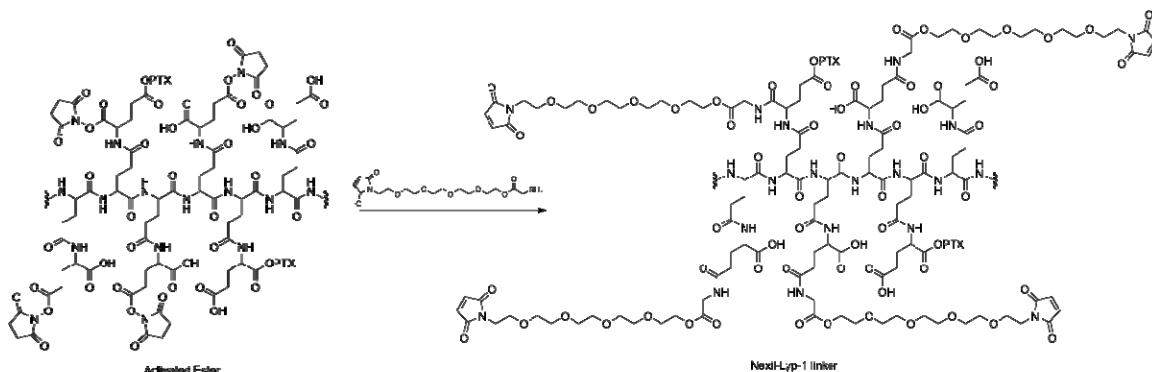
Scheme 2

In a round bottom flask at room temperature and under argon atmosphere the material obtained in the previous reaction (activated Nexil) was dissolved in dry DMF and to this solution the Lyp-1 linker was added. The reaction was stirred at room temperature during approximately 36 hours. After this time the reaction was quenched adding cold Et₂O promoting the precipitation of the polymer. The suspension was transferred to a centrifuge tube and the sample was centrifuged at 10˚C during 10 minutes at 3600 rpm. The solvent was removed and the precipitated was transferred to a round bottom flask and dry in high vacuum pump overnight. The ^{1}H NMR spectrum shows the characteristic peak of the maleimide group at 7.02 ppm apart from the resonance of the PEG protons between 3.4-3.7 ppm.

Second Step- Nexil-Lyp-1 linker peptide coupling reaction
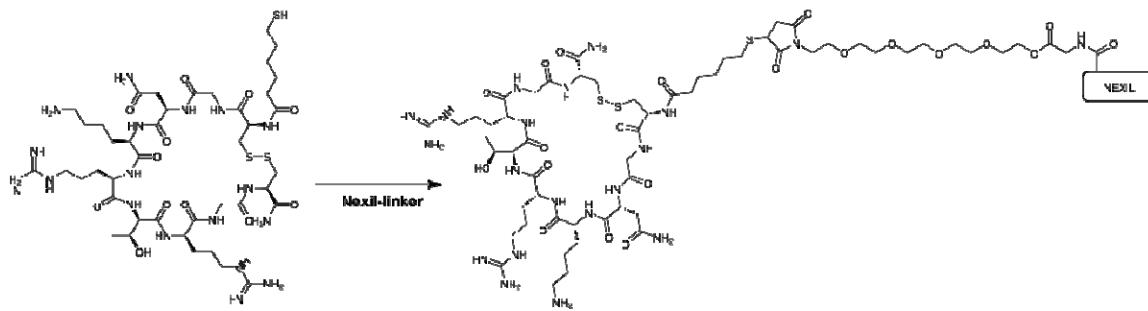
Scheme 3

In a round bottom flask the Nexil-Lyp-1 linker (50 mg) was dissolved in DMSO (2 mL) and to this solution it was added PBS buffer pH 7 (1mL). The Lyp-1 peptide (50mg) was added to this solution and reaction was stirred overnight at room temperature. The reaction was quenched adding water and the solution became cloudy (it is very likely that the Nexil-Lyp-1 conjugate it is not hydrophilic enough to bring the compound into solution in the acidic form). The compound was transferred to a dialysis bag and dialyzed overnight. The compound was lyophilized and analyzed by NMR. A small sample of the compound obtained was dissolved in deutered DMSO and ^{1}H NMR spectrum was taken. Unfortunately in this first attempt it was not possible to make sure the desired compound was obtained.

In order to optimize the reaction conditions for this coupling, it was tested under conditions where only the Lyp-1 peptide and linker were included in the reaction. The advantage of using these compounds is the simple analysis of the reaction outcome by analytical HPLC. The reaction conditions were similar to the one described previously, but acetonitrile instead of DMSO was used. One aliquot from the reaction was taken after two hours and injected in the HPLC revealing the reaction completion. This approach also failed to generate the desired product. A major effort has subsequently been made during the last year of this grant, and the no cost extension to complete the synthesis of Lyp-1 linked to Nexil. Multiple additional conditions were tested using both the approach of adding the linker first to the Nexil polymer and then adding the Lyp-1, and the approach of adding the linker first to the Lyp-1 and then coupling the Lyp-1-linker to the polymer. Some of the conditions tested yielded small amounts of product, but we were unable to identify either an approach, or conditions for a given approach, that allowed the isolation and purification of sufficient Lyp-1-linker-Nexil for testing of its activity against human ovarian cancer cells either in vitro or in vivo. It should be noted that the Lyp-1 peptide has features that limit the types of chemical approaches that can be used when coupling to a polymer, and that several other laboratories have also failed in attempts to produce Lyp-1 coupled to either polymers or particles in amount sufficient for animal testing.

1. Evaluation of CPE as a targeting peptide

As we began to appreciate that the chemistry of linking Lyp-1 to Nexil was going to be more difficult than anticipated, we turned substantial attention to the identification of additional peptides that could target drugs to ovarian cancers. One peptide of interest is the CPE-C, a 30 amino acid peptide derived from the C-terminal end of *Clostridium perfringens* enterotoxin. Claudins are the major integral membrane proteins forming the backbone of tight junctions between epithelial cells. These proteins can form homodimers or heterodimers to produce paired strands connecting adjacent cells, thereby determining the characteristic permeability properties of different epithelial tissues [16]. Using gene expression profiling, we and others have found that claudin-3 (*CLDN3*) and claudin-4 (*CLDN4*) genes are highly expressed in ovarian cancers [17-19]. In addition, several other studies have reported aberrant claudin expression in various cancers. These two genes are not normally highly expressed in non-malignant human tissues including the normal ovarian epithelium [20], clearly associating abundance of these two proteins with malignancy.

Although the exact role that *CLDN3* and *CLDN4* over-expression plays in ovarian cancer is still unclear, these tight junction proteins have recently been shown to be the naturally-occurring receptors for *Clostridium perfringens* enterotoxin (CPE), a single polypeptide with a molecular mass of 35 kDa that causes the symptoms associated with *Clostridium perfringens* food poisoning [21]. Among more than 20 members of claudin family, CLDN3 and CLDN4 are the only transmembrane tissue-specific claudin proteins capable of mediating CPE binding and cytolysis [22]. Analysis of the CPE structure-function relationship through characterization of the functional properties of enterotoxin fragments has revealed that the C-terminal 30 amino acid fragment of CPE (CPE$_{290-319}$) does not cause cytolysis but retains high affinity binding to the claudins (Ka = 1.49 x 10^{-8} M^{-1}). This fragment also completely blocks specific binding of the full-length toxin thus abolishing cytolysis of susceptible target cells [21, 23]. Furthermore, CPE$_{290-319}$ has shown no immunogenicity [23]. These findings suggest that the CPE peptide fragment might serve to target cytotoxins claudins on various ovarian cancers that express high levels of CLDN3 and CLDN4. Previous studies from this laboratory had demonstrated that CPE could be fused with TNF, and that this fusion protein could selectively kill ovarian carcinoma cells that express CLDN3 or CLDN4 [24]. However, TNF turned out not to be very potent when tested in vivo. In seeking to further explore the potential of CPE as a tumor-target peptide we have now fused CPE to the more potent toxin gelonin.

Construction, expression and purification of rGel-based fusion proteins.

As illustrated in Fig.12A, the initial rGel-based fusion toxins consisted of a flexible G_4S linker tethering the C-terminus of $CPE_{290-319}$ to the N-terminus of rGel. The 30 amino acid $CPE_{290-319}$ peptide is abbreviated in this paper as "CPE". The CPE-G_4S-rGel construct was further engineered by replacing G_4S with the furin-cleavable cell-penetrating sequence R_9 to make CPE-R_9-rGel. Vectors expressing other variants containing combinations of CPE, E_9, G_4S and R_9 were constructed by splicing overlap extension PCR (SOE-PCR). Each contained an N-terminal histidine tag to assist purification followed by a SUMO protease cleavage site that allowed subsequent removal of the histidine tag. Following expression in *E. coli*, purification and SUMO cleavage to remove the 6×His tag, the final purified products of all the rGel-based fusion toxins migrated on SDS-PAGE at the expected molecular weights of 28.2, 31.9, 33.0, 29.6, 31.3, and 34.4 kDa, respectively, for rGel, CPE-G_4S-rGel, CPE-R_9-rGel, R_9-rGel, E_9-G_4S-R_9-rGel and CPE-E_9-G_4S-R_9-rGel (Fig. 10B).


Figure 12. Preparation of rGel-based series fusion toxins. A. Schematic diagram of the fusion constructs containing CPE, E_9, R_9 and rGel. B. SDS-PAGE analysis of the final purified products of the above toxins.

Binding activity

To ensure that the CPE-containing fusion toxins retained receptor binding, their ability to bind to a human ovarian carcinoma cell line was assessed using an ELISA-based binding assay (Fig. 12A). The 2008 ovarian cancer cell line expresses both CLDN3 and CLDN4, and we have previously reported on the subline 2008-CLDN3KD-4.5, in which the expression of CLDN3 was knocked down using a lentiviral vector expressing a short hairpin RNA targeted to CLDN3 mRNA [24]. These isogenic CLDN3-positive and negative cells were exposed to graded concentrations of the fusion toxins, after washing the binding was assessed by determining the amount of cell-bound toxin by reaction with an anti-rGel antibody. Equilibrium dissociation constants were calculated using GraphPad Prism, v4.03. The affinity of CPE-G_4S-rGel, CPE-R_9-rGel, and CPE-E_9-G_4S-R_9-rGel for CLDN-positive 2008 cells was similar with a K_d value of 13.63, 14.73 and 10.57 nmol/L, respectively. The K_d values are consistent with a previous report (Ka = 1.49×10^8 M^{-1}) based on an ^{125}I-CPE saturation binding assay [21]. In contrast, the binding of CPE-containing toxins to CLDN3-knockdown cells was markedly reduced (Fig. 12B) suggesting that the binding specificity is dependent on the expression of the claudin receptors on the tumor cell membrane.
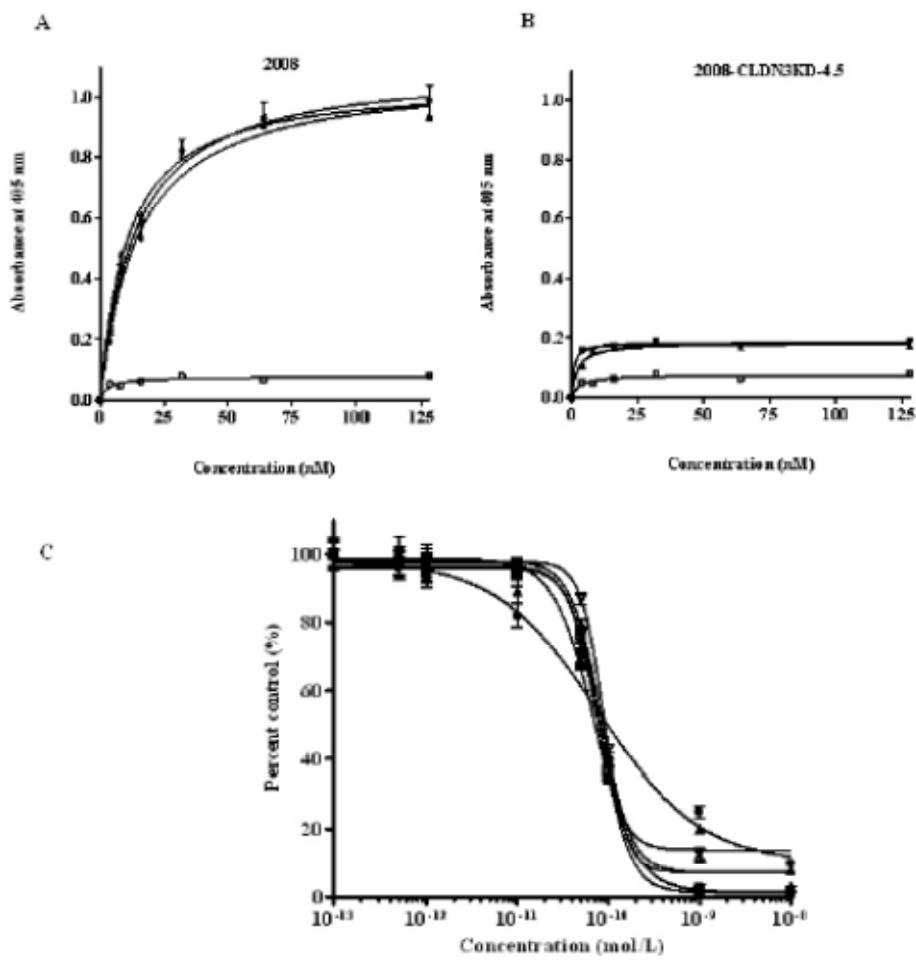
Figure 13. *Characterization and comparison of rGel-based fusion toxins.* **A.** *Evaluation of the binding of the fusion constructs CPE-G$_4$S-rGel (▼), CPE-R$_9$-rGel (●), CPE-E$_9$-G$_4$S-R$_9$-rGel (▲) and rGel (□) to 2008 cells by whole-cell ELISA.* **B.** *Evaluation of the binding of the fusion constructs CPE-G$_4$S-rGel (▼), CPE-R$_9$-rGel (●), CPE-E$_9$-G$_4$S-R$_9$-rGel (▲) and rGel (□) to 2008-CLDN3KD-4.5 cells by whole-cell ELISA.* **C.** *The enzymatic (N-glycosidase) activity of the rGel component of the fusions (■, rGel; ▲, CPE-G$_4$S-rGel; ●, CPE-R$_9$-rGel; □, R$_9$-rGel; Δ, E$_9$-G$_4$S-R$_9$-rGel; ∇, CPE-E$_9$-G$_4$S-R$_9$-rGel) as assessed using rabbit reticulocyte lysate assay.*

Protein synthesis inhibitory activity

The biological activity of toxins can be severely compromised when incorporated into fusion constructs. To examine the N-glycosidic activity of the rGel component of the fusion toxins, these materials were added to an *in vitro* protein translation assay in which [^{3}H] leucine is incorporated into isolated rabbit reticulocytes. Inhibition curves for the fusion constructs CPE-G$_4$S-rGel, CPE-R$_9$-rGel, R$_9$-rGel, E$_9$-G$_4$S-R$_9$-rGel and CPE-E$_9$-G$_4$S-R$_9$-rGel were compared to that of native rGel. As shown in Fig. 13 C, the IC$_{50}$ values for the six molecules were found to be virtually identical (71.2, 71.6, 75.6, 81.0, 82.2, 88.4 pmol/L, respectively, for rGel, CPE-G$_4$S-rGel, CPE-R$_9$-rGel, R$_9$-rGel, E$_9$-G$_4$S-R$_9$-rGel and CPE-E$_9$-G$_4$S-R$_9$-rGel) although the shape of the inhibition curve for CPE-R$_9$-rGel was slightly different from the others indicating that no loss of toxin activity occurred as a result of fusing rGel to the targeting moieties.
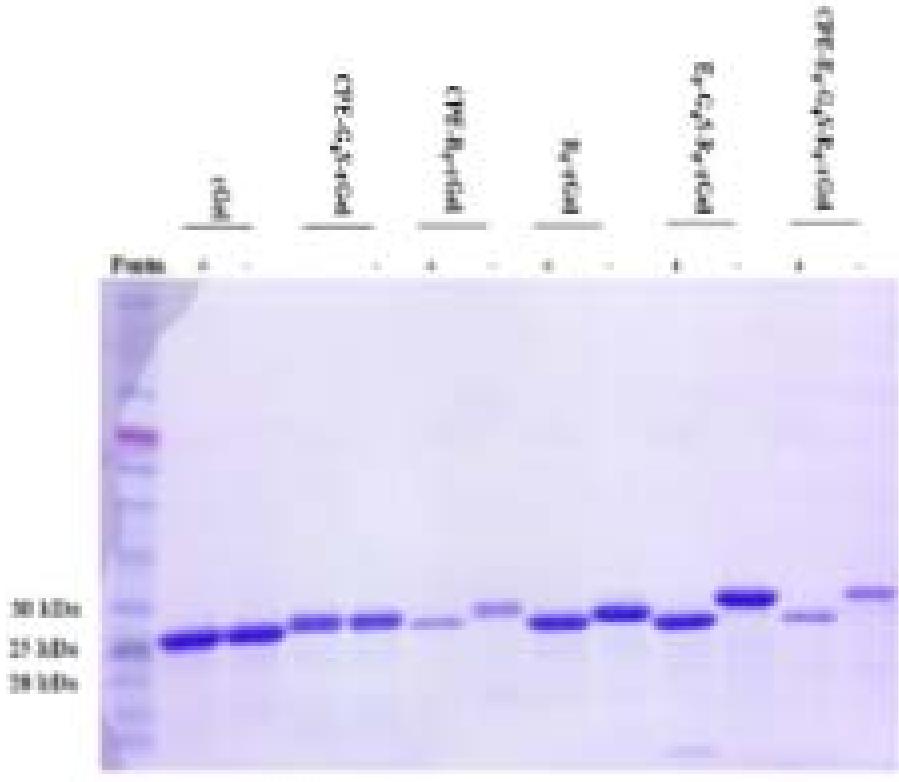
Figure 14. SDS-PAGE analysis of in vitro furin cleavage of rGel-based fusion toxins. Purified proteins were incubated with recombinant furin at room temperature for 16 h at pH 7.2.

In vitro cleavage of rGel-based toxins by furin

To investigate the susceptibility of various chimeric toxins to proteolytic cleavage, the purified fusion proteins were subjected to proteolysis with recombinant furin in a physiological buffer at pH 7.2. As shown in Fig. 14, CPE-R_9-rGel, R_9-rGel, E_9-G_4S-R_9-rGel and CPE-E_9-G_4S-R_9-rGel were all cleaved efficiently. In contrast, CPE-G_4S-rGel, in which CPE is fused with rGel through a G_4S linker was not cleaved. Thus, the R_9 linker was sensitive to furin cleavage even at pH 7.2 whereas the G_4S was found to be resistant to the action of this protease.

Stability analysis and cellular uptake of rGel-based toxins

Stability of various rGel fusion constructs in tissue culture medium and their subsequent intracellular accumulation after endocytosis was assessed by Western blot analysis using an anti-rGel antibody (Fig. 14). The rGel fusion peptides were added to 2008 cells growing in RPMI medium containing 5% fetal bovine serum for a period of 6 h at a concentration of 1 μM, all the fusion proteins stayed largely intact in the medium without significant degradation suggesting that little or no proteolytic cleavage occurred outside the cultured cells. However, only CPE-R_9-rGel and R_9-rGel were detected inside the cells after a 6 h exposure indicating that R_9 promotes cellular uptake of the cargo molecule. This result indicates that, in the absence of the charge neutralization provided by the E_9, the R_9 moiety markedly enhances the cellular accumulation of rGel, but that addition of the E9 sequence is quite effective at blocking this effect. Of note is the fact that the vast majority of the intracellular rGel remained undegraded.

Cellular accumulation of the various fusion proteins was also analyzed by immunofluorescent staining (Fig. 15B). The ovarian 2008 cells were exposed to each test protein at a concentration of 250 nM for 6 h at 37 °C and, following fixation, they were stained with an anti-gelonin antibody followed by a secondary Texas red-conjugated antibody prior to examination on a deconvoluting microscope. Fig. 15B shows the relative amount and intracellular distribution of rGel following incubation with rGel, CPE-G_4S-rGel, and R_9-rGel. Control cells not exposed to any of the proteins showed no intracellular staining (data not shown), as was also the case for

18

cells exposed to rGel. Cells exposed to CPE-G$_4$S-rGel contained a small amount of dispersed punctuate intracellular staining suggestive of localization within vesicular structures. In contrast, extensive diffuse intracellular staining indicative of cytosolic localization was observed in the cells exposed to R$_9$-rGel. Thus, as detected by the immunofluorescent staining, CPE was able to enhance the cellular accumulation of rGel despite the fact that this could not be detected by Western blot analysis. However, consistent with the Western blot analysis, CPE was far less effective than the R$_9$ moiety.
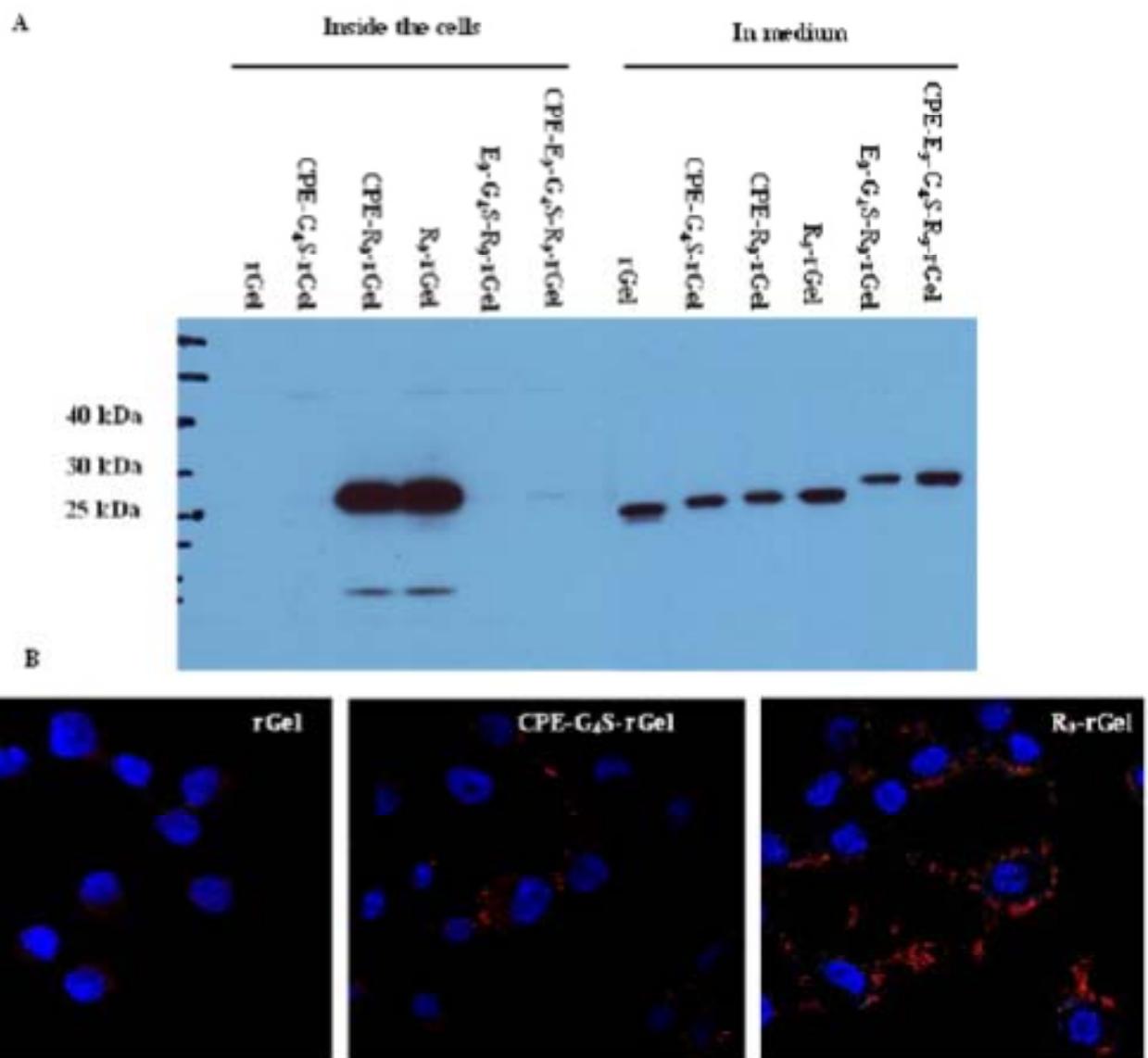
*Figure 15. Stability analysis and intracellular uptake of rGel fusion toxins. **A.** Extent of degradation following exposure of 1 μM to 2008 cells for 6 h. The medium and cells were subjected to Western blot analysis with anti-rGel antibody. **B.** Internalization of rGel, CPE-G$_4$S-rGel and R$_9$-rGel into 2008 cells. Cells were treated with 250 nM of each fusion toxin for 6 h and stained with rabbit anti-gelonin antibody and Texas red-coupled anti-rabbit secondary antibody. Nuclei were stained with Hoechst 33342 (blue).*

In vitro cytotoxicity

The cytotoxicity of the various fusion proteins was assessed by testing their ability to slow the growth of the 2008 cells. Cells were cultured for 72 h with increasing concentrations of each purified fusion protein and the percent survival in comparison to controls treated only with phosphate buffered saline was determined in CCK-8 assays. As shown in Fig. 16A, despite the ability of the CPE peptide to enhance rGel uptake as detected

by the immunofluorescent staining, CPE-G$_4$S-rGel produced no greater reduction in survival than rGel itself. This indicates that the additional amount of rGel brought into the cell through the interaction of CPE with claudins 3 and 4 was sequestered in an intracellular compartment from which it could not escape to reach the ribosome and inhibit protein synthesis.

Strikingly, when the R$_9$ moiety was added to the fusion protein it enhanced cell killing 10-fold over that attained with CPE-G$_4$S-rGel alone (IC$_{50}$ 78 nM versus 715 nM). To determine whether the enhanced cytotoxic activity of CPE-R$_9$-rGel was still dependent on the specific binding of CPE to the claudin receptors on the cell surface, R$_9$-rGel was included in the cytotoxicity study. Intriguingly, R$_9$-rGel without the CPE targeting moiety displayed even more potent cell killing with an IC$_{50}$ of 38 nM. This is consistent with the well known ability of arginine-rich peptides to efficiently translocate cargo through cell membranes. However, the addition of the R$_9$ moiety clearly did not assist in the goal of achieving claudin-dependent cytotoxicity.
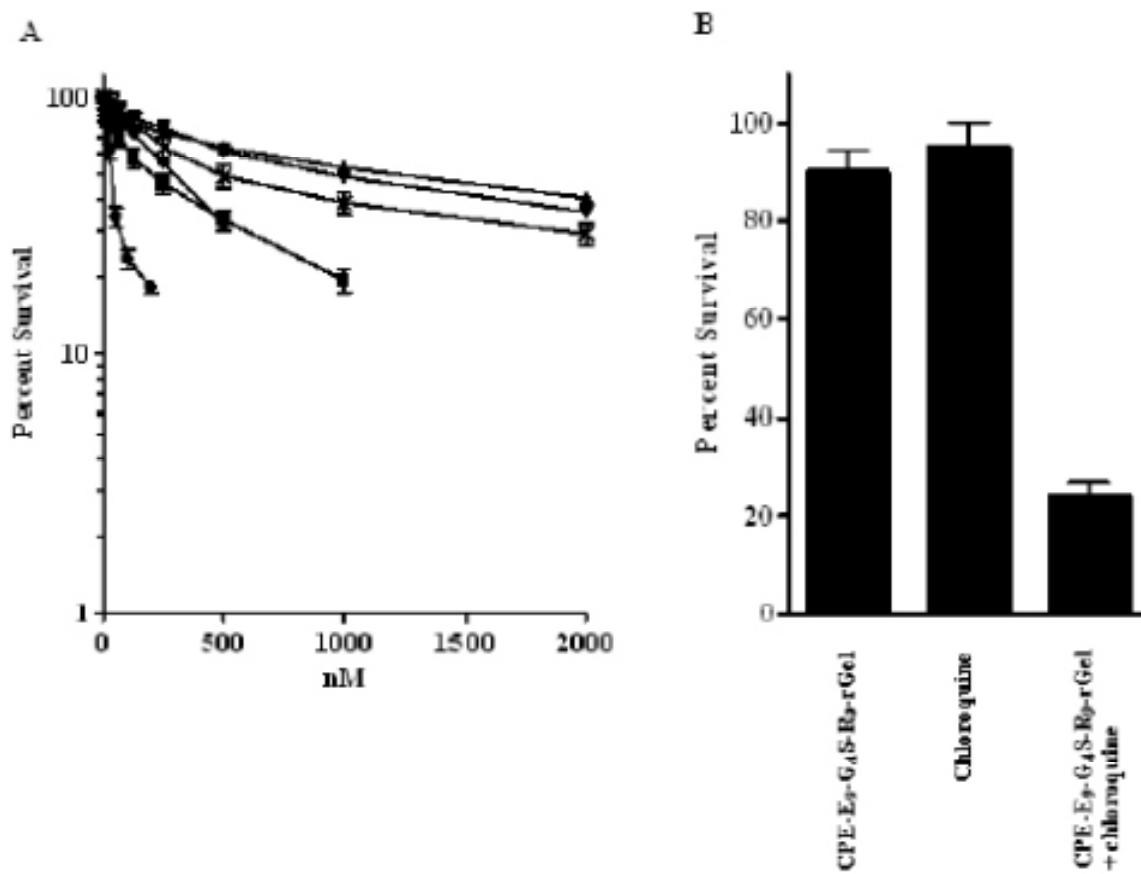
Figure 16. *Cytotoxicity of rGel-based fusion toxins. A. In vitro cytotoxicity of various rGel-based series fusion toxins against 2008 cells (▲,rGel; ▼, CPE-G$_4$S-rGel; ●, R$_9$-rGel; ♦, CPE-R$_9$-rGel; ■, E$_9$-G$_4$S-R$_9$-rGel ; and ✕, CPE-E$_9$-G$_4$S-R$_9$-rGel). B. Enhancement of the cytotoxicity of CPE-E$_9$-G$_4$S-R$_9$-rGel to 2008 cells by the endosomolytic reagent chloroquine. Cells were treated with 31.25 nM CPE-E$_9$-G$_4$S-R$_9$-rGel for 6 h, washed with complete medium 3 times and subsequently incubated with 50 μM chloroquine for 16 h. Afterwards, the chloroquine-containing medium was also removed and replaced with fresh growth medium after 3 times washing. The cytotoxic effects were determined by CCK-8 assay at 72 h after exposure to CPE-E$_9$-G$_4$S-R$_9$-rGel.*

Neutralization of R9 to enhance specificity

Given that the R_9 moiety was so effective at enhancing uptake, we reasoned that it would likely also be good at releasing rGel from the compartment into which CPE delivered it. However, to make use of the R_9 sequence in this manner it is necessary to mask the R_9 until after CPE-mediated and claudin-dependent endocytotic uptake. The addition of a 9 poly-glutamic acid sequence (E_9) to the R_9 moiety so as to neutralize its positive charge has previously been shown to disable the ability of R_9 to enter cells [25]. We explored the use of this approach to block R_9 non-specific cell membrane penetration until the toxin had undergone internalization mediated by the ligand-receptor binding and ended up in endosomes. The first step was to prove that E_9 could in fact mask the cell-penetrating capacity of the R9 in 2008 cells. To this end an E_9-G_4S-R_9-rGel fusion protein was produced and tested for cytotoxicity. The addition of the E_9 through a G_4S linker to R_9-rGel increased the IC_{50} by 5.3-fold from 38 nM to 202 nM indicating that the inhibitory E_9 domain can largely neutralize the R_9 domain (Fig. 16A). Addition of CPE to the E_9-G_4S-R_9-rGel fusion protein further reduced the IC_{50} to 482 nM consistent with the concept that the CPE directs the CPE-E_9-G_4S-R_9-rGel to intracellular vesicles from which it has difficulty escaping. To confirm this, the 2008 cells were incubated with an IC_{10} concentration of CPE-E_9-G_4S-R_9-rGel (31.25 nM) for 6 h and then exposed to a non-toxic concentration (50 uM) of the endosomolytic reagent chloroquine for 16 h. As shown in Fig. 16B, addition of chloroquine increased the inhibition of growth produced by this concentration of CPE-E_9-G_4S-R_9-rGel from 10% to 76%. Thus, CPE provides targeting to claudin-expressing tumor cells, R_9 provides a mechanism for getting out of intracellular compartment, and E_9 offers an approach to masking the non-specific toxicity of R_9-rGel. However, a mechanism for cleaving the CPE-E_9 fragment from the R_9-rGel fragment once inside the cell is still needed.

Protease-dependent cleavage

One approach to separating CPE-E_9 from R_9-rGel after endocytosis is to introduce a sequence between the E_9 and R_9 that is cleavable by a protease found in the compartment into which CPE sequesters the fusion protein. Despite the fact that the R_9 sequence is itself a substrate for the endosomal/lysosomal protease furin, clearly this reaction was insufficient to release significant amounts of R_9-rGel. To this end, a series of fusion proteins were produced containing sequences previously reported to be substrates for various endosomal/lysosomal proteases. In an attempt to make the R9 sequence itself a better protease substrate the R9 was modified to the optimum furin-cleavable sequence RRKRRRRRR. In a second attempt, the G_4S linker was replaced with a GFLG sequence that is cleavable by endosomal cathepsin B. Finally, both were introduced into a third version of the fusion protein as CPE-E_9-GFLG-R_2KR_6-rGel. However, when tested against 2008 cells, none of these further modifications significantly enhanced the cytotoxicity of the CPE-E_9-G_4S-R_9-rGel. We then tried inserting a 10-residue furin cleavable sequence from the diphtheria toxin translocation domain (A_{187}GNRVRRSVG$_{196}$, Fdt) between the CPE fragment and the rGel. A recombinant immunoproapoptotic protein containing this sequence was previously shown to result in more potent cell killing activity than those with other furin-sensitive sequences [26]. However, introduction of the Fdt sequence previously reported to enhance endosomal escape also failed to enhance the cytotoxicity of CPE-rGel.

CPE was fused to rGel at its N-terminal end via a flexible G_4S linker. This CPE-G_4S-rGel molecule was internalized into vesicles from which location it produced little cytotoxicity. To enhance release from the endosomal/lysosomal compartment a poly-arginine sequence (R_9) was introduced between the CPE and the rGel. CPE-R_9-rGel was 10-fold more cytotoxic but selectivity for claudin-expressing cells was lost. The addition of a poly-glutamic acid sequence (E_9) through a G_4S linker to R_9-rGel (E_9-G_4S-R_9-rGel) largely neutralized the non-selective cell membrane penetrating activity of the R_9 motif. However, introduction of CPE to the E_9-G_4S-R_9-rGel fusion protein (CPE-E_9-G_4S-R_9-rGel) further reduced its cytotoxic effect. Treatment with the endosomolytic reagent chloroquine increased the cytotoxicity of CPE-E_9-G_4S-R_9-rGel. Several types of linkers susceptible to cleavage by furin and endosomal cathepsin B were tested for their ability to enhance R_9-rGel release but none of these modifications further enhanced the cytotoxicity of CPE-E_9-G_4S-R_9-rGel. We concluded that while a claudin-3 and -4 ligand serves to deliver rGel into 2008 cells the delivered molecules were entrapped in intracellular vesicles. Incorporation of R_9 non-specifically increased rGel cytotoxicity and this effect could be masked by inclusion of an E9 sequence. However, the putative protease cleavable sequences

tested were inadequate for release of R_9-rGel from CPE-E_9-G_4S-R_9-rGel. This work has now been published [27].

3. Evaluation of A6 as a targeting peptide

During the no cost extension period of this grant we turned attention to the question of whether the A6 peptide could be used to target drug loaded polymers to tumors. A6 is an eight amino acid peptide (acetyl-KPSSPPEE-amino) that has been shown to have anti-invasive, anti-migratory and anti-angiogenic activities in a variety of in vitro and in vivo model systems [28-30]. Short peptides like A6 with unique biologic activities are emerging as potential targeting moieties for many types of cancer. CD44 is a heavily glycosylated membrane protein that functions in cell-cell and cell-matrix adhesion and is a marker of stem cells in several types of tumors. The amino acid sequence of A6 exhibits marked homology with a linear sequence within CD44. The homologous sequence (120-NASAPPEE-127) resides within the HA-binding domain of CD44 in an exposed linker between two β strands. The A6-like sequence is present in all isoforms of CD44 and straddles the splice junction between standard exons 3 and 4. The asparagine residue, a potential N-glycosylation site, is located two residues carboxyl from a cysteine residue that is part of a disulfide bond that is critical for conformational integrity of CD44 and its ability to bind HA. Thus, the A6-like sequence in CD44 appears to be located within a region of the ligand binding domain that is structurally important and potentially conformationally dynamic.

Given the importance of CD44 as a potential target, and the established biological activities of A6 we sought to determine whether A6 really targeted CD44. We found that A6 inhibited the migration of a subset of ovarian and breast cancer cell lines, exhibiting IC_{50} values of 5-110 nM. There was an association between the potency of A6 in the migration assay and the expression of CD44. We found that A6 could be crosslinked to CD44 and that immunoprecipitation of CD44 brought down A6. We also found that when A6 bound to CD44 it altered the structure of the receptor such that it could not be recognized by a monoclonal antibody to a specific epitope. The binding of A6 to CD44 affected downstream signaling from CD44 and activated focal adhesion kinase and MEK phosphorylation. We concluded that A6 binds to CD44 receptor, and that it appears to be a good candidate for use as a targeting peptide for the development of polymer or nanoparticle based drug delivery systems.

KEY RESEARCH ACCOMPLISHMENTS

- Established a clear correlation between the amount of the Nexil polymer backbone and paclitaxel that accumulated in the
- Demonstrated that addition of RGD to the Nexil polymer did not significantly enhance activity in a xenograft model
- Established a synthetic route for the production of Lyp-1 and successfully synthesized Lyp-1 coupled to two different length linkers but we were unable to find a way of combining the Lyp-1, the linker and the Nexil in a manner that yielded sufficient product for further testing.
- Showed that CPE can target the toxin gelonin to claudin-3 and claudin-4 on ovarian cancer cells but that much of the toxin become sequestered into endosomal compartments from which release is limited.
- Documented the ability of the A6 peptide to bind to the CD44 receptor and qualified it as a candidate tumor-targeting peptide

REPORTABLE OUTCOMES

Presentations

None

Abstracts

Lin, X, Yuan, X, Manorek, G, Howell, SB, Targeted delivery of gelonin to claudin-expressing cancer cells and use of activatable cell penetrating peptides to enhance potency, Abstract #3627. Published in Proc. Am. Assn Cancer Res 52:867, 2011

Manuscripts

Yuan, X., Lin X., Manorek, G., Howell, S.B., Challenges associated with the targeted delivery of gelonin to claudin-expressing cancer cells with the use of activatable cell penetrating peptides to enhance potency. BMC Cancer 11:61, 2011. PMID: 21303546 PMCID: PMC3042419

CONCLUSIONS

We have established that there is an excellent correlation between the tumor uptake of Nexil and its ability to deliver paclitaxel in a panel of 8 human tumor xenografts. In addition to facilitating the pharmacokinetic analysis of various forms of peptide-target Nexil the results of these experiments provide a strong rationale for the development of Nexil-DTPA as an agent for selection of patients to be enrolled on Nexil clinical trials in the future.

Although we successfully synthesized RGD-target Nexil we were unable to show improved efficacy in a lung cancer mode.

A great deal of effort has gone in to developing routes for the synthesis of Lyp-1, the linkers needed to couple it to Nexil and the Lyp-1-linker complex. After what appeared to be initial success with the production of small batches, we have subsequently been unable to reproducibly generate the product in amounts large enough for testing in animals.

We have shown that the CPE peptide effectively targets the toxin gelonin to human ovarian cancer cells in a claudin-dependent manner, but that this fusion molecule has a difficult time getting out of the endosomal compartment and reaching the ribosome which is the target of gelonin.

We have identified the A6 peptide as being able to bind to the CD44 receptor which is a marker of tumor stem cells, and have qualified it as a tumor-targeting peptide worthy of further study.

REFERENCES

1.   Wang, X., et al., *Pharmacokinetics and tissue distribution of PGG-paclitaxel, a novel macromolecular formulation of paclitaxel, in nu/nu mice bearing NCI-460 lung cancer xenografts.* Cancer Chemother Pharmacol, 2010. 65(3): p. 515-26.
2.   Feng, Z., et al., *Preclinical efficacy studies of a novel nanoparticle-based formulation of paclitaxel that out-performs Abraxane.* Cancer Chemother Pharmacol, 2009. 65: p. 923-930
3.   Ferrari, M., *Cancer nanotechnology: opportunities and challenges.* Nat Rev Cancer, 2005. 5(3): p. 161-71.
4.   Duncan, R., *The dawning era of polymer therapeutics.* Nat Rev Drug Discov, 2003. 2(5): p. 347-60.
5.   Allen, T.M. and P.R. Cullis, *Drug delivery systems: entering the mainstream.* Science, 2004. 303(5665): p. 1818-22.
6.   Peer, D., et al., *Nanocarriers as an emerging platform for cancer therapy.* Nat Nanotechnol, 2007. 2(12): p. 751-60.
7.   Li, C., et al., *Complete regression of well-established tumors using a novel water-soluble poly(L-glutamic acid)-paclitaxel conjugate.* Cancer Res, 1998. 58(11): p. 2404-9.

8. Van, S., et al., *Synthesis, characterization, and biological evaluation of poly(L-gamma-glutamyl-glutamine)- paclitaxel nanoconjugate.* Int J Nanomedicine, 2010. 5: p. 825-37.

9. Sugahara, K.N., et al., *Tissue-penetrating delivery of compounds and nanoparticles into tumors.* Cancer Cell, 2009. 16(6): p. 510-20.

10. Laakkonen, P., et al., *A tumor-homing peptide with a targeting specificity related to lymphatic vessels.* Nat Med, 2002. 8(7): p. 751-5.

11. Laakkonen, P., et al., *Antitumor activity of a homing peptide that targets tumor lymphatics and tumor cells.* Proc Natl Acad Sci U S A, 2004. 101(25): p. 9381-6.

12. Fogal, V., et al., *Mitochondrial/cell-surface protein p32/gC1qR as a molecular target in tumor cells and tumor stroma.* Cancer Res, 2008. 68(17): p. 7210-8.

13. von Maltzahn, G., et al., *In vivo tumor cell targeting with "click" nanoparticles.* Bioconjug Chem, 2008. 19(8): p. 1570-8.

14. Karmali, P.P., et al., *Targeting of albumin-embedded paclitaxel nanoparticles to tumors.* Nanomedicine, 2009. 5(1): p. 73-82.

15. Makela, A.R., et al., *Tumor targeting of baculovirus displaying a lymphatic homing peptide.* J Gene Med, 2008. 10(9): p. 1019-31.

16. Sasaki, H., et al., *Dynamic behavior of paired claudin strands within apposing plasma membranes.* Proc Natl Acad Sci U S A, 2003. 100(7): p. 3971-6.

17. Cheng, T.C., et al., *Identification of genes whose expression is associated with cisplatin resistance in human ovarian carcinoma cells.* Cancer Chemother Pharmacol, 2006. 58(3): p. 384-95.

18. Hough, C.D., et al., *Large-scale serial analysis of gene expression reveals genes differentially expressed in ovarian cancer.* Cancer Res, 2000. 60(22): p. 6281-7.

19. Lu, K.H., et al., *Selection of potential markers for epithelial ovarian cancer with gene expression arrays and recursive descent partition analysis.* Clin Cancer Res, 2004. 10(10): p. 3291-300.

20. Rangel, L.B., et al., *Tight junction proteins claudin-3 and claudin-4 are frequently overexpressed in ovarian cancer but not in ovarian cystadenomas.* Clin Cancer Res, 2003. 9(7): p. 2567-75.

21. Katahira, J., et al., *Molecular cloning and functional characterization of the receptor for Clostridium perfringens enterotoxin.* J Cell Biol, 1997. 136(6): p. 1239-47.

22. Katahira, J., et al., *Clostridium perfringens enterotoxin utilizes two structurally related membrane proteins as functional receptors in vivo.* J Biol Chem, 1997. 272(42): p. 26652-8.

23. Hanna, P.C., et al., *Localization of the receptor-binding region of Clostridium perfringens enterotoxin utilizing cloned toxin fragments and synthetic peptides. The 30 C-terminal amino acids define a functional binding region.* J Biol Chem, 1991. 266(17): p. 11037-43.

24. Yuan, X., et al., *Recombinant CPE fused to tumor necrosis factor targets human ovarian cancer cells expressing the claudin-3 and claudin-4 receptors.* Mol Cancer Ther, 2009. 8(7): p. 1906-15.

25. Jiang, T., et al., *Tumor imaging by means of proteolytic activation of cell-penetrating peptides.* Proc Natl Acad Sci U S A, 2004. 101(51): p. 17867-72.

26. Wang, T., et al., *Recombinant immunoproapoptotic proteins with furin site can translocate and kill HER2-positive cancer cells.* Cancer Res, 2007. 67(24): p. 11830-9.

27. Yuan, X., et al., *Challenges associated with the targeted delivery of gelonin to claudin-expressing cancer cells with the use of activatable cell penetrating peptides to enhance potency.* BMC Cancer, 2011. 11: p. 61.

28. Guo, Y., et al., *An antiangiogenic urokinase-derived peptide combined with tamoxifen decreases tumor growth and metastasis in a syngeneic model of breast cancer.* Cancer Res, 2002. 62(16): p. 4678-84.

29. Boyd, D.D., et al., *A urokinase-derived peptide (A6) increases survival of mice bearing orthotopically grown prostate cancer and reduces lymph node metastasis.* Am J Pathol, 2003. 162(2): p. 619-26.

30. Mishima, K., et al., *A peptide derived from the non-receptor-binding region of urokinase plasminogen activator inhibits glioblastoma growth and angiogenesis in vivo in combination with cisplatin.* Proc Natl Acad Sci U S A, 2000. 97(15): p. 8484-9.